Input-Current Addition in Closely Positioned Dual-Stage Ballistic Rectifiers

J. von Pock, U. Wieser, and U. Kunze*

Werkstoffe und Nanoelektronik, Ruhr-Universität Bochum, D-44780 Bochum, Germany

(Received 17 January 2017; revised manuscript received 3 April 2017; published 27 April 2017)

Injection-type ballistic rectifiers are realized as asymmetric cross junctions. Their output-voltage (V_{out}) input-current (I_{in}) characteristics are known as parabola $V_{\mathrm{out}} = \alpha^2 I_{\mathrm{in}}^2$, where α^2 is the curvature coefficient. Previous experiments on widely separated dual-stage ballistic rectifiers yielded the total output signal to be the sum of that of the single stages $V_{\mathrm{out}} = \alpha_1^2 I_{\mathrm{in1}}^2 + \alpha_2^2 I_{\mathrm{in2}}^2$. Starting from an ostensive model containing the ballistic length as critical size, we show that sufficiently closely positioned stages lead to input-current addition $V_{\mathrm{out}} = (\alpha_1 I_{\mathrm{in1}} + \alpha_2 I_{\mathrm{in2}})^2$. We demonstrate two consequences of current addition. First, the excess voltage with respect to voltage addition $V_{\mathrm{exc}} = 2\alpha_1\alpha_2 I_{\mathrm{in1}} I_{\mathrm{in2}}$ is proportional to the product $I_{\mathrm{in1}} I_{\mathrm{in2}}$. Second, sign-dependent current cancellation results in a shift of the $V_{\mathrm{out}}(I_{\mathrm{in1}})$ parabola vertex at fixed I_{in2} or, at $I_{\mathrm{in1}} = -I_{\mathrm{in2}}$, to vanishing output voltage. The regime of intermediate-stage separation is discussed in terms of partial overlap of the injected charge clouds, leading to a smaller excess voltage. The results should provide both a deeper insight into the microscopic mechanism of ballistic rectification and novel device applications.

DOI: 10.1103/PhysRevApplied.7.044023

I. INTRODUCTION

Electron transport in semiconductors is determined by a number of characteristic lengths. If critical device dimensions become comparable to or smaller than a characteristic length, novel effects emerge, which can be exploited in device applications. A prominent device is the bipolar transistor [1], where the thickness of the neutral base must be smaller than the diffusion length of the minority carriers [2]. A more recent example is the Aharonov-Bohm effect [3], which arises in one-dimensional (1D) quantum ring structures with path lengths smaller than the wave-function coherence length [4,5]. In the present work we investigate ballistic rectifiers, which are realized as asymmetric cross junctions of current-carrying injector and current-free voltage channels. Symmetry breaking has been initially implemented by an asymmetric antidot scatterer at the center of an orthogonal cross junction forming a reflection-type rectifier [6]. Our concept of an injection-type rectifier employs a noncentrosymmetric cross junction, where the current-injecting leads are inclined by an angle $\phi < 90°$ with respect to the voltage channel [7–9]. In the nonlinear ballistic transport regime, the asymmetric current channel guides the ballistic electron trajectories into the same current-free voltage lead independent of the current polarity. As a result, the voltage channel (stem) is stationary charged and a nonlocal voltage develops across the stem, which represents a full-wave rectification. Note that trajectory guiding requires a width of the cross junction which is smaller than the ballistic length of the charge carriers. A particular advantage of ballistic rectifiers is a roughly parabolic output-voltage-vs-input-current transfer characteristic leading to zero cut-in voltage [8], unlike conventional rectifier barrier diodes. However, the output voltage is extremely small, impeding a practical application. A method to increase the voltage relies on connecting two or more rectifier stages in series [10]. Closely located stages are expected to have a mutual impact on their transfer characteristics because the injected charge clouds are extended on a scale given by the ballistic length of the electrons, which at low temperatures is known to be smaller than the mean free path [11]. In the following consideration we outline the influence of the interstage separation on the transfer characteristics, which we expect as a result of at least partly overlapping charge clouds injected by the injector pairs.

II. CURRENT-ADDITION MODEL

Figure 1(a) represents a schematic of a two-stage ballistic rectifier. The current is injected from the leads (1,2) and/or (3,4) and the output voltage arises between the upper (U) and lower (L) lead. Upon driving one of the injector pairs, the output voltage is proportional to the current square, i.e., $V_{UL}^{ij} = \alpha_{ij}^2 I_{ij}^2$, where ij refers to the respective contacts (1,2) or (3,4), and α_{ij}^2 represents the individual curvature coefficients. Because of the large separation, both rectifier stages are independent from each other, thus when driving both stages their output voltages add up to the total output voltage $V_{UL}^{12,34} = V_{UL}^{12} + V_{UL}^{34}$, as observed earlier [10]. However, in the limit of vanishing separation [Fig. 1(b)] where both injector pairs would connect the stem exactly at the same position (which is practically impossible) the injected charge clouds completely overlap each other. Since the electrons in the clouds do not remember from which

*Corresponding author.
ulrich.kunze@rub.de

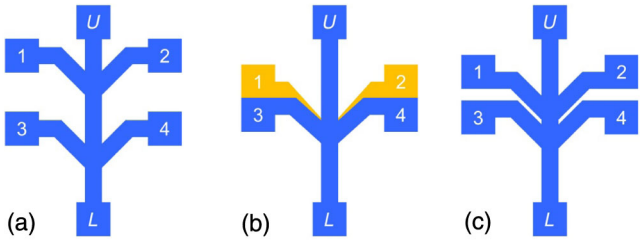

FIG. 1. Virtual two-stage ballistic rectifiers for different injection conditions. Leads (1,2) and (3,4) denote the current-injecting channels, the upper (U) and lower (L) contacts represent the output of the rectified dc voltage. (a) A separation between stages much larger than the ballistic length results in nonoverlapping injected charge clouds. (b) Vanishing separation leads to completely overlapping clouds. (c) If the separation is finite but still smaller than the ballistic length, the charge clouds partially overlap each other.

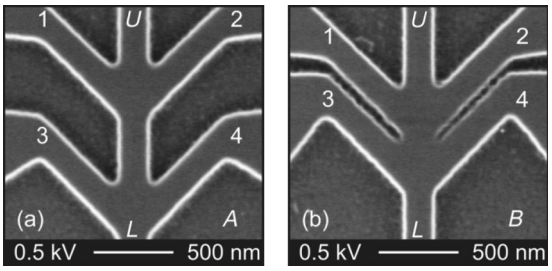

FIG. 2. Scanning electron microscopy (SEM) picture of (a) device A and (b) device B before depositing the global metal gate. The conducting channels and contact areas are defined by 45-nm-deep etching, which depletes the 60-nm-deep 2DEG. The injector and the voltage leads merge under an angle of 45°. The width of the injector and voltage channels is $w \sim 190$ nm. The center-to-center distance between the injectors (1,3) amounts to $d_{13} \sim 740$ nm and $d_{13} \sim 340$ nm for devices A and B, respectively.

injector they have been injected, the same situation should be present if only one injector pair would be driven by the sum of both currents. Therefore, the injection by two injector pairs of zero distance can be viewed as pure current addition leading to $V_{UL}^{12,34} = (\alpha_{12} I_{12} + \alpha_{34} I_{34})^2$, which exceeds $V_{UL}^{12,34} = V_{UL}^{12} + V_{UL}^{34}$ valid for pure voltage addition at large injector separation. For equal curvatures ($\alpha_{12} = \alpha_{34}$) the same signal also should arise if the total current $I_{12} + I_{34}$ is injected into one of the injector pairs, however, their maximum current is limited by carrier heating. Our interpretation suggests that the excess voltage $V_{UL}^{\mathrm{exc}} = V_{UL}^{12,34} - V_{UL}^{12} - V_{UL}^{34}$ can be read as a mixed term in $V_{UL}^{12,34}$, i.e., $V_{UL}^{\mathrm{exc}} = 2\beta\alpha_{12}\alpha_{34} I_{12} I_{34}$, where β describes the degree of overlap between the injected charge clouds $0 \le \beta \le 1$. An intermediate situation may be present if the stages are spatially separated by less than the ballistic length, as depicted in Fig. 1(c).

In the present work we describe experiments on two-stage ballistic rectifiers where the distance between the current injectors is varied. At particularly small stage separation, the results completely confirm the current-addition model. We expect that current addition makes an impact on the development of multistage ballistic rectifier devices suitable for technical applications. Also, current addition may provide a deeper insight into the microscopic model for ballistic rectification, which so far is still unsatisfactory.

III. SAMPLE DESIGN AND FABRICATION

Motivated by the predictions of the current-addition model we fabricate two-stage rectifiers with $\phi = 45°$ as shown in Fig. 2. In addition to widely spaced stages as in Fig. 2(a) we also try to position both stages as close as possible, as depicted in Fig. 2(b). The samples are based on a modulation-doped Si/SiGe heterostructure where the two-dimensional electron gas (2DEG) is 60 nm below the surface. The electron mobility is $\mu = 18.3\ \mathrm{m^2\,V^{-1}\,s^{-1}}$ ($1.9\ \mathrm{m^2\,V^{-1}\,s^{-1}}$) at $T = 1.4$ K (77 K) and the density $n_S = 6.3 \times 10^{15}\ \mathrm{m^{-2}}$ ($6.6 \times 10^{15}\ \mathrm{m^{-2}}$), which leads to a mean free path of $\ell_e \sim 1.7\ \mu$m ($0.2\ \mu$m), respectively. The geometric width of 200 nm is reduced by a lateral depletion width of about 35 nm, which provides smooth edges and, hence, favors ballistic transport. Owing to the large electron density of the heterostructure, the remaining electrical channel width proves to be sufficient to endure injection currents in excess of 10 μA [8]. Accepting a nominal width $w = 190$ nm and a lithographic minimum width of about $g = 50$ nm for an etched groove isolating neighboring channels, the minimum separation between the injector pairs (1,2) and (3,4) can be estimated as $d_{13,\mathrm{min}} = (w + g)/\sin\phi$. For an injection angle of $\phi = 45°$ the result is $d_{13,\mathrm{min}} \sim 340$ nm in accordance with the separation d_{13} obtained in device B [Fig. 1(b)]. This separation should be compared with the ballistic length ℓ_b of the injected electrons. Even if no experiments are available which properly determine ℓ_b in a Si/SiGe 2DEG, an estimation is possible from ballistic rectifiers on this material having the 2DEG 30 nm below the surface and a mean free path of $\ell_e \sim 0.55\ \mu$m at $T = 1.5$ K [12]. An injection-type rectifier on this material having a voltage channel width of $w = 275$ nm shows ballistic rectification, while for $w = 550$ nm the ballistic signal is absent. For the present material this indicates $275\ \mathrm{nm} < \ell_b < \ell_e \sim 1.7\ \mu$m, which should be sufficiently large.

Sample preparation is performed using low-energy electron-beam lithography and low-damage reactive ion etching as described in Ref. [12]. Note that the lateral definition of the geometry is determined not only by the process resolution of about 30 nm but also by the lateral depletion width. The electrical characterization is performed by driving the injector pairs of contacts 1–2 and 3–4 independently by current sources (realized by voltage sources with respect to ground and 1-$M\Omega$ series

resistances) while measuring the output voltage V_{UL}. A configuration in push-pull fashion ($I_{12} = -I_{21}$ and $I_{34} = -I_{43}$) ensures a minimum change of the potential at the junction center, i.e., the effective gate voltage is kept constant. The global top gate is biased from threshold voltage $V_{\rm th}$, which is approximately -1.0 V, up to $V_g = +0.2$ V, where the gate leakage current is negligibly small ($I_g < 1$ nA). A gate voltage $V_g = +0.2$ V is sufficiently large for widely suppressing contributions from hot-electron thermopower [9]. Unless otherwise noted the measurements are performed at $T = 4.2$ K.

IV. RESULTS AND DISCUSSION

Figure 3 displays the transfer characteristics of the individual rectifier stages and for equal currents in both stages. These characteristics roughly exhibit a parabolic behavior which is typical for ballistic rectifiers [7–9]. For device A with large distance between the injector pairs, for both stages the curvature coefficients are $\alpha_{12}^2 = (1.44 \pm 0.01) \times 10^7$ V/A^2 and $\alpha_{34}^2 = (1.56 \pm 0.02) \times 10^7$ V/A^2, which is about the same as for single-stage rectifiers having the same geometry [8]. In two-stage operation under $I_{12} = I_{34}$, which corresponds to the numerical addition of the individual output voltages V_{UL}^{ij}, the total output voltage adds up to the same value, $V_{UL}^{12,34} = V_{UL}^{12} + V_{UL}^{34}$ [Fig. 3(a)] as observed earlier for much larger devices [10]. At smaller injector separation, as shown in Fig. 3(b) for device B, the curvature coefficients amount to $\alpha_{12}^2 = (5.05 \pm 0.09) \times 10^6$ V/A^2 and $\alpha_{34}^2 = (3.57 \pm 0.09) \times 10^6$ V/A^2, which is smaller than for the large-distance device A by a factor of about 0.3. This may be an effect of mutual disturbing of the potential landscape defining the asymmetric cross junctions [13]. The mutual disturbance is not assumed to arise from worsened reflections of injected electrons at the channel boundaries, because this would only affect the electrons injected from the upper stage (1,2) and not for those of the lower stage (3,4). We suppose that the potential landscape is disturbed by the potential minima formed by the wider space at the centers of the cross junctions. Unfortunately, a corresponding examination of single-stage ballistic rectifiers with a locally widened channel closely spaced to the cross junction is still missing. However, $V_{UL}^{12,34}$ exceeds the sum $V_{UL}^{12} + V_{UL}^{34}$ by a factor of 2 as expected from the current-addition model for a total overlap of the charge clouds ($\beta = 1$). This indicates that the stage separation of device B is smaller than the ballistic length.

The current-addition model predicts a proportionality of the measured $V_{UL}^{\rm exc}$ to the product $I_{12}I_{34}$. This is illustrated by a series of measurements of device B as shown in Fig. 4(a), where the ratio I_{12}/I_{34} is fixed in a range of $0.1 \le I_{12}/I_{34} \le 10$ and $V_{UL}^{\rm exc} = V_{UL}^{12,34} - V_{UL}^{12} - V_{UL}^{34}$ is plotted as a function of $I_{12}I_{34}$. Since the transfer characteristics are slightly asymmetric, $V_{UL}^{\rm exc}$ represents the average for positive and negative currents. The merging of all measurement data in Fig. 4(a) into the same straight line confirms the current-addition model. The slope of the line is proportional to the overlap coefficient according to $V_{UL}^{\rm exc}/(I_{12}I_{34}) = 2\beta\alpha_{12}\alpha_{34}$, hence the coefficient can be calculated as $\beta = V_{UL}^{\rm exc}/[2(V_{UL}^{12}V_{UL}^{34})^{1/2}]$. A different approach which eliminates any distortion by the asymmetry of the individual transfer characteristics started from calculating the curvature coefficients α_{12} and α_{34} by a least-square fit to the parabolic parts of V_{UL}^{12} and V_{UL}^{34}. In the same way the excess-voltage coefficient $\alpha_{\rm exc}$ is evaluated from the two-stage measurements ($I_{12} = I_{34} = I$), where $V_{UL}^{\rm exc} = \alpha_{\rm exc} I^2$, and finally the overlap coefficient is extracted as $\beta = \alpha_{\rm exc}/(2\alpha_{12}\alpha_{34})$. The result is $\beta_A = 0.00 \pm 0.02$ and $\beta_B = 1.02 \pm 0.06$ for devices A and B, respectively. Measurements at excited temperatures revealed constant coefficients up to $T = 50$ K. We conclude that even up to $T = 50$ K the ballistic length is larger than the separation between the stages of device B.

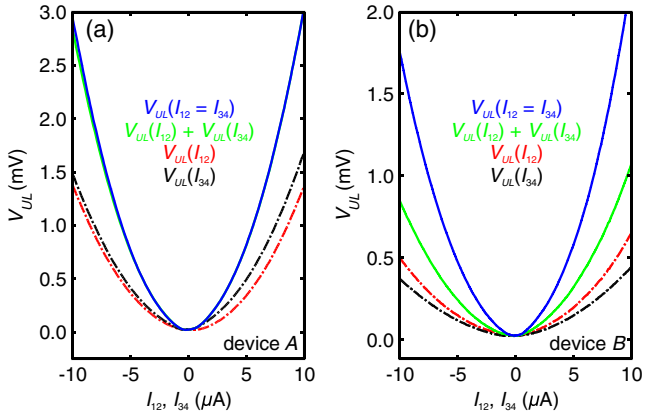

FIG. 3 (a) Transfer characteristics of device A at gate voltage $V_g = +0.2$ V. The characteristics are measured for the individual stages $V_{UL}^{12}(I_{12})$ and $V_{UL}^{34}(I_{34})$, and for two-stage operation under equal currents $V_{UL}^{12,34}(I_{12} = I_{34})$, and compared with the calculated sum $V_{UL}^{12} + V_{UL}^{34}$. (b) Corresponding results as in (a) for the device B, $V_g = +0.2$ V. Note that $V_{UL}^{12,34} > V_{UL}^{12} + V_{UL}^{34}$ arising from the smaller separation d_{13}.

If one of the injector currents is fixed, e.g., $I_{34} = \text{const}$, the current-addition model predicts a shift of the $V_{UL}^{12,34}$-vs-I_{12} parabola vertex along the current axis to $I_{12,\rm min} = -\beta(\alpha_{34}/\alpha_{12})I_{34}$ and a raise to $V_{UL,\rm min}^{12,34} = \alpha_{34}^2 I_{34}^2(1-\beta^2)$. For $\beta = 0$ both stages are decoupled, therefore the parabola remains centered at $I_{12,\rm min} = 0$ and raised by the contribution of the second stage to $V_{UL,\rm min}^{12,34} = \alpha_{34}^2 I_{34}^2$, as shown in Fig. 4(b). For $\beta = 1$ both currents compensate each other at $I_{12,\rm min} = -(\alpha_{34}/\alpha_{12})I_{34}$ forming a zero in the voltage signal $V_{UL,\rm min}^{12,34} = 0$, as depicted in Fig. 4(c). Incomplete current addition causes a vertex shift to finite I_{12} and $V_{\rm UL}$. Also, driving the stages by equal currents of opposite polarity ($I_{34} = -I_{12} = -I$) is correctly described by the

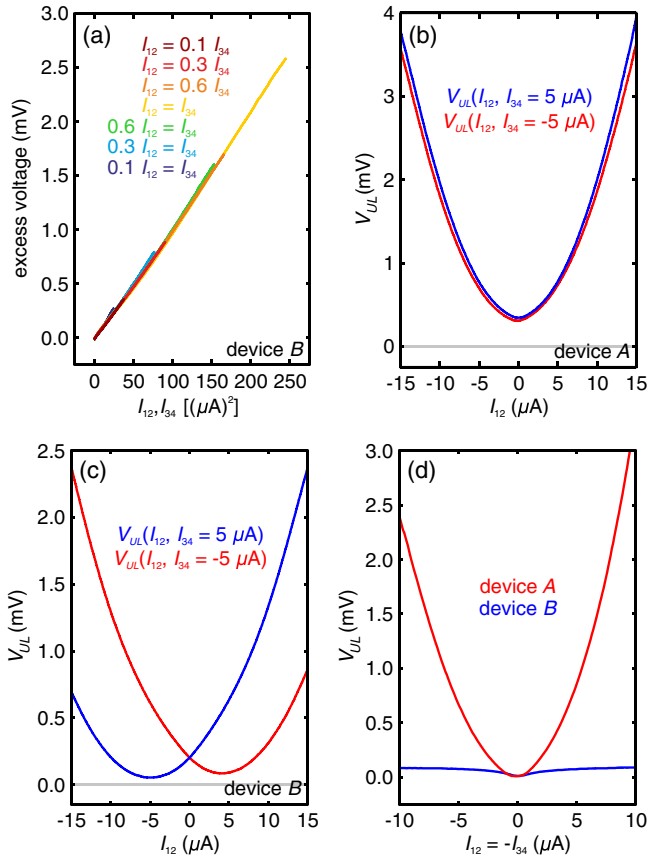

FIG. 4. (a) Excess voltage $V_{UL}^{\mathrm{exc}} = V_{UL}^{12,34} - V_{UL}^{12} - V_{UL}^{34}$ of device B as a function of the current product $I_{12}I_{34}$ for different ratios I_{12}/I_{34}. Straight lines support a model that assumes virtual current addition. Note that the measurement range is limited by maximum currents of about 16 μA. (b),(c) Transfer characteristics of the respective devices A and B for a fixed current in the lower stage, $I_{34} = \pm 5\ \mu$A, while I_{12} is varied ($V_g = +0.2$ V). (d) Characteristics for varying both I_{12} and I_{34} at $I_{12} = -I_{34}$. Device A ($V_g = +0.2$ V) yields a voltage addition as in Fig. 2(a), $V_{UL}^{12,34}(I_{12} = -I_{34}) = V_{UL}^{12,34}(I_{12} = I_{34})$. For device B ($V_g = +0.2$ V) the result should be $V_{UL}^{12,34}(I_{12} = -I_{34}) = 0$ if $\alpha_{12} = \alpha_{34}$.

model as $V_{UL}^{12,34} = (\alpha_{12}^2 + \alpha_{34}^2 - 2\beta\alpha_{12}\alpha_{34})I^2$, hence we get voltage addition for device A ($\beta = 0$) and nearly vanishing output voltage for device B ($\beta = 1$), see Fig. 4(d). We would also like to mention that additional measurements using voltage sources instead of current sources, again applied in push-pull fashion ($V_2 = -V_1$), give the same results as those shown in Figs. 3 and 4. The voltage that is required to drive a current of $|I| = 10\ \mu$A amounts to $|V_2 - V_1| \sim 40$ mV.

In addition to the experiments described so far, we also characterize a device C having the same geometry as devices A and B except for the separation between the injector leads, which is somewhat larger than in device B, namely $d_{13} \sim 390$ nm. Here, the transfer characteristics of the individual stages and for two-stage operation (not shown) reveal an excess voltage of about 60%, indicating partial overlap of the injected charge clouds. The corresponding overlap coefficient amounts to $\beta_C = 0.82 \pm 0.18$. Obviously, the ballistic length dominating the transfer characteristics of dual-stage ballistic rectifiers on the used Si/SiGe material amounts to $\ell_b \sim 400$ nm.

So far, we have stressed the importance of the ballistic length compared with the stage separation. The concept of the ballistic length was initially developed in the semiclassical billiard model as an average momentum decay length for electrons whose trajectories are controlled by external electric and magnetic fields in the near-equilibrium transport [14]. Because of current heating, the injected electrons gain excess energy, which is transferred to the lattice by phonon emission, hence the ballistic length decreases as current is increased. In principle, if the excess energy reaches the threshold TA phonon energy of 19 meV in Si ballistic transport effects break down [15], which is not observed here. Electron excess energy also gives rise to inelastic electron-electron (e-e) scattering, which destroys the ballistic motion of the individual charge carriers [11] and, thus, converts the transport process from the ballistic into the drift-diffusion regime. This is the reason why at low temperatures diffusion hot-electron thermopower is observed in the transfer characteristics of ballistic rectifiers even over large distances where the ballistic signal vanishes [12]. Importantly, e-e scattering (without umklapp processes) is momentum conserving for the whole electron ensemble [16]. The corresponding momentum decay length is still compatible with the current-addition model for two-stage ballistic rectifiers. Also, electrons coming from different stages are able to interact without disturbing their contribution to the collective momentum, while in the billiard model mutual interactions may be viewed as destructive events for the ballistic motion.

V. CONCLUDING REMARKS

A technical aspect of current instead of voltage addition is the improved efficiency, which may reduce the number of stages required to get an output voltage of technical relevance while avoiding sufficiently large stage separations for minimizing mutual disturbance. This is particularly important for a large number of stages necessary to achieve an output voltage approaching the input voltage. Once a better material enables room-temperature operation of a ballistic rectifier [17–19], current addition may be a key ingredient for developing the semiconductor nanostructure into a different type of nanoscale electronic device. A unique aspect arises from sign-sensitive current addition as shown in Fig. 4(c), which indicates that one of the stages can be used to control the transfer characteristic of the other one. Also, the $I_{12}I_{34}$ term of the excess voltage suggests the application as a mixer, which should be useful up to THz frequencies owing to the small parasitic capacitances of the lateral device structure.

ACKNOWLEDGMENTS

We are grateful to T. Hackbarth for growing the Si/SiGe heterostructures and to A. Wiggershaus for phosphorus implantation.

[1] J. Bardeen and W. H. Brattain, The transistor, a semiconductor triode, Phys. Rev. **74**, 230 (1948).
[2] W. Shockley, The theory of *p-n* junctions in semiconductors and *p-n* junction transistors, Bell Syst. Tech. J. **28**, 435 (1949).
[3] Y. Aharonov and D. Bohm, Significance of electromagnetic potentials in the quantum theory, Phys. Rev. **115**, 485 (1959).
[4] G. Timp, A. M. Chang, J. E. Cunningham, T. Y. Chang, P. Mankiewich, R. Behringer, and R. E. Howard, Observation of the Aharonov-Bohm Effect for $\omega_c\tau > 1$, Phys. Rev. Lett. **58**, 2814 (1987).
[5] S. S. Buchholz, S. F. Fischer, U. Kunze, M. Bell, D. Reuter, and A. D. Wieck, Control of the transmission phase in an asymmetric four-terminal Aharonov-Bohm interferometer, Phys. Rev. B **82**, 045432 (2010).
[6] A. M. Song, A. Lorke, A. Kriele, J. P. Kotthaus, W. Wegscheider, and M. Bichler, Nonlinear Electron Transport in an Asymmetric Microjunction: A Ballistic Rectifier, Phys. Rev. Lett. **80**, 3831 (1998).
[7] M. Knop, U. Wieser, U. Kunze, D. Reuter, and A. D. Wieck, Ballistic rectification in an asymmetric mesoscopic cross junction, Appl. Phys. Lett. **88**, 082110 (2006).
[8] D. Salloch, U. Wieser, U. Kunze, and T. Hackbarth, Thermopower-enhanced efficiency of Si/SiGe ballistic rectifiers, Appl. Phys. Lett. **94**, 203503 (2009).
[9] J. F. von Pock, D. Salloch, U. Wieser, T. Hackbarth, and U. Kunze, Identification and separation of rectifier mechanisms in Si/SiGe ballistic cross junctions, J. Appl. Phys. **121**, 014304 (2017).
[10] U. Wieser, M. Knop, P. Koop, U. Kunze, D. Reuter, and A. D. Wieck, Enhanced rectification efficiency in cascaded ballistic GaAs/AlGaAs rectifiers, AIP Conf. Proc. **893**, 719 (2007).
[11] R. I. Hornsey, J. R. A. Cleaver, and H. Ahmed, Transverse hot-electron electron focusing, Phys. Rev. B **48**, 14679 (1993).
[12] D. Salloch, U. Wieser, U. Kunze, and T. Hackbarth, Influence of channel width on the performance of an injection-type ballistic rectifier: Carrier injection versus hot-electron thermopower, Microelectron. Eng. **88**, 2386 (2011).
[13] This result is confirmed by a total number of 4 (10) devices having closely (distantly) arranged stages, respectively.
[14] C. W. J. Beenakker and H. van Houten, Billiard Model of a Ballistic Multiprobe Conductor, Phys. Rev. Lett. **63**, 1857 (1989).
[15] U. Wieser, S. A. Poenariu, U. Kunze, and T. Hackbarth, Phonon-induced breakdown of negative bend resistance in an asymmetric Si/SiGe cross junction, Appl. Phys. Lett. **87**, 252114 (2005).
[16] R. N. Gurzhi, Hydrodynamic effects in solids at low temperatures, Sov. Phys. Usp. **11**, 255 (1968).
[17] A. M. Gilbertson, A. Kormányos, P. D. Buckle, M. Fearn, T. Ashley, C. J. Lambert, S. A. Solin, and L. F. Cohen, Room temperature ballistic transport in InSb quantum well nanodevices, Appl. Phys. Lett. **99**, 242101 (2011).
[18] E. Matioli and T. Palacios, Room-temperature ballistic transport in III-nitride heterostructures, Nano Lett. **15**, 1070 (2015).
[19] G. Auton, J. Zhang, R. K. Kumar, H. Wang, X. Zhang, Q. Wang, E. Hill, and A. Song, Graphene ballistic nanorectifier with very high responsivity, Nat. Commun. **7**, 11670 (2016).